Open Access

Femtosecond Laser-Induced Nanowelding: Fundamentals and Applications

A. Hu[*,1], Y. Zhou[1] and W.W. Duley[2]

[1]*Centre for Advanced Material Joining, Department of Mechanical and Mechatronics Engineering, University of Waterloo, Canada*

[2]*Department of Physics, University of Waterloo, 200 Univ. Ave. West, Waterloo, ON N2L 3G1, Canada*

Abstract: Fundamentals of femtosecond laser pulse and nanoparticles are analyzed by a two-temperature model. Ultrafast surface melting, surface nanoengineering and shock wave impact are evident in the surface of graphite by femtosecond irradiation. The interaction between femtosecond laser pulses and Au/Ag nanoparticles has been investigated. Two effects are identified at different intensities: photofragmentation at rather high intensity (~10^{14} W/cm^2), nanojoining at low intensity (~10^{10}W/cm^2). Photofragmentation forms a large number of tiny nanoparticles with an average size of tens of nanometers. Control over irradiation conditions at intensities near 10^{10} W/cm^2 results in nanojoining of most of the nanoparticles. This nanojoining is obtained in both liquid solution and in solid state thin films assembled from nanoparticles. Nanojoining mechanism is further studied by joining Ag nanoparticles encapsulated by a polymer shell. Nonthermal melting is investigated. Nanojoined Au nanoparticles are expected to have numerous applications, such as probes for surface enhance Raman spectroscopy.

Keywords: Femtosecond laser irradiation, nanowelding, two-temperature model, raman spectroscopy.

1. INTRODUCTION

Nanomaterials present unique electric, magnetic, catalytic and optical properties different from their bulk materials due to the quantum size effect, nanostructure and shape [1-3] and the explosive expansion of applications in various fields such as electronics, health care, energy generation, and storage [2-4]. According to BCC research, the global market for nanomaterials in biomedical, pharmaceutical, and cosmetic applications has an estimated scale of $ 0.2 billion in 2007 and is expected to suppress $ 0.68 billion by 2012, corresponding to a compound average annual growth rate of 27.3% [5]. Nanomaterials are also generating comprehensive implications on the development of science and playing a central role in the emerging technological revolution, e.g. metal nanoparticles are pushing optics past the diffraction limit and fully into the nanosized regime [6]. The science and technology that investigate the excitation, control, manipulation and propagation of surface plasmon has recently developed into an independent research field known as "plasmonics" [2]. The research in this field has diverse applications in surface enhanced spectroscopy, near-field optical microscopy with unprecedented resolution, manipulation of light signals and novel negative refraction materials for superlensing [2, 7]. Extensive biomedical applications of nanomaterials have created innovative technologies in genomics, biosensing, immunoassays, clinical diagnostics, cancer cell photothermolysis, drug delivery [3]. Recently, the application of ultrafast laser to nanomaterials has led to a cutting edge field, namely, ultrafast nano-optics [4], which focuses on elementary physical processes, electron and energy transport in polymer and large bio-molecules, electron quantum transport phenomena, and surface plasmon dynamics in metal and semiconductor nanostructures.

It is important to point out that nanojoining has to develop in order to build and assemble functional nano-devices with dissimilar nano- and/or molecular components. Also, nanojoining allows nanodevices integrating with micro-and macrosystem and surrounding. It is long known that welding and joining is an essential step in the fabrication of various devices at different scales including macro, micro and nano. As devices become increasingly smaller, challenges faced in micro and nano-joining must be overcome before these joints are safely implemented. For example, researchers must determine how to robustly join these miniature building blocks while avoiding excessive damage. When the building blocks shrink into submicro or even to a range of nanometers, such as the fabrication of nanomechanical engineering systems (NEMS), the melting has to be controlled within the thickness of a few nanometers. Ultrafast pulsed laser is an innovative tool in this field for nanoscopic processing [8]. Femtosecond laser irradiation can result in an ultrafast and nonthermal melting of solid materials, which is promising for developing novel joining technologies for nano- and/or molecular devices. With the development of nanoscience and technology, nanoscopic joining technologies are gaining more significance [9, 10].

In this review paper we discussed the interaction fundamentals between ultrafast laser and matter. We presented the detailed results of experiments on the application of femtoseond laser for nonthermal nanowelding. Then, we demonstrated the application of welded nanoparticles for the surface enhanced Raman spectroscopy.

*Address correspondence to this author at the Centre for Advanced Materials Joining, University of Waterloo, 200 University Avenue West, Waterloo, Ontario, N2L 3G1, Canada, Tel: 519-8884567-35464.
E-mail: a2hu@uwaterloo.ca

Finally, we draw the conclusions and gave the outlook of this research field.

2. FUNDAMENTALS OF FEMTOSECOND LASER-INDUCED NANOWELDING

2.1. Interaction Between fs Laser Pulses and Matter: General Picture

The primary laser-solid interaction process involves the excitation of electrons from their equilibrium states to higher energy levels by photo absorption. For example, in semiconductors electrons can be excited from the valence band to the conduction band by single or multi-photon absorption.

At a given laser fluence $F \propto I\tau$, a shorter pulse duration favors multiphoton excitation because the probability of nonlinear absorption increases strongly with laser intensity. Different interactions have been discussed by von der Linde *et al.* [11] with increasing pulse widths.

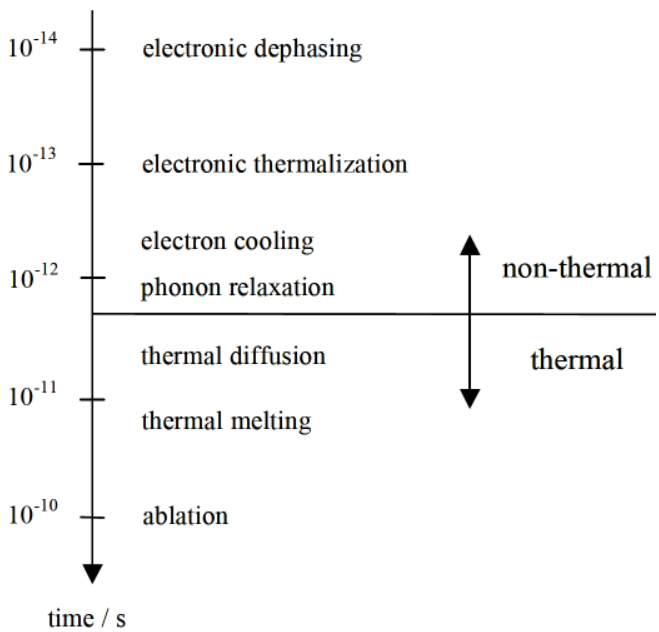

Fig. (1). Time scale for various secondary processes in laser-matter interactions [11].

As shown in Fig. (**1**), a very short-lived transient coherent polarization is associated with a primary electronic excitation. This polarization is destroyed by a de-phasing process occurring at a time scale of 10 fs. The initial distribution of excited electronic states corresponds to the coupling states of optical transitions. The occupation of these primary states is subsequently changed by nonthermal carrier-carrier Coulomb interaction on a time scale of about 100 fs. The hot electron state can be further cooled by emission of phonons. Electron cooling and phonon relaxation occur in < 1 ps.

Thermal cooling occurs on time scales > 1 ps. Heat diffusion occurs by electron-lattice interactions and by phonon coupling. The lattice thermal melting is longer than 10 ps while ablation occurs during the laser pulse. Thus, the interaction between intense laser radiation and matter can be modeled by a two-temperature theory in which electrons and lattice remain at different temperatures.

2.2. Two-Temperature Model

According to a one-dimensional, two temperature diffusion model [12, 13], the energy of low intensity short laser pulses is absorbed by free electrons due to inverse Bremsstrahlung (Joule heat). The evolution of the absorbed energy involves thermalization within the electron gas (electron subsystem), energy transfer to the lattice and thermal diffusion in the lattice. These processes can be expressed as:

$$C_e \frac{\partial T_e}{\partial t} = -\frac{\partial Q(z)}{\partial z} - \gamma(T_e - T_i) + S\,, \tag{1.1}$$

$$C_i \frac{\partial T_i}{\partial t} = \gamma(T_e - T_i)\,, \tag{1.2}$$

$$Q(z) = -k_e \partial T_e / \partial z\,,\ S = I(t) A\alpha \exp(-\alpha z) \tag{1.3}$$

Here z is the direction of energy propagation perpendicular to the target surface, $Q(z)$ is the heat flux, S is the laser source function, I(t) the laser intensity, $A=1-R$ is the surface transmissivity and α is the absorption coefficient. C_e and C_i are the specific heat of the electron and lattice subsystems with $C_e = aT_e$ where a is a constant, γ is the electron-lattice coupling parameter, and k_e is electron thermal conductivity.

In eq. (1.1-3) we should consider three characteristic time scales: τ_e, τ_i, and τ_L. $\tau_e = C_e/\gamma$ is the electron cooling time, $\tau_i = C_i/\gamma$ is the lattice heating time or the characteristic thermal diffusion time and τ_L the laser pulse width. Following previous studies [11, 14, 15], the laser pulses can be separated into three time regimes.

2.2.1. Ultrafast Pulses in a Femtosecond Scale

For a fs pulse, the laser width is much shorter than the electron cooling time, $\tau_L << \tau_e \sim 1ps$. Then, $C_e T_e / t >> \gamma T_e$, and electron-lattice coupling can be neglected. This means that there is no energy transfer from the electron to the lattice. If $D_e \tau_L < \alpha^{-2}$, where $D_e = k_e/C_e$ is the electron thermal diffusivity, the electron heat conduction term can be neglected and eq. (1.2) reduces to

$$C_e^{'} \partial T_e^2 / \partial t = 2 I_a \alpha \exp(-\alpha z) \tag{1.4}$$

and gives

$$T_e(t) = (T_o^2 + \frac{2 I_a \alpha}{C_e^{'}} t \exp(-\alpha z))^{1/2}\,. \tag{1.5}$$

Here it is assumed that I(t) = I_o and $I_a = I_o A$, while $T_o = T_e(0)$ is the initial temperature of the material. $C_e^{'} = C_e / T_e$ is a constant when T_e remains smaller than the Fermi energy (in temperature). At the end of the laser pulse the electron temperature is given by

$$T_e(\tau_L) \cong (\frac{2 F_a \alpha}{C_e^{'}})^{1/2} \exp(-z/\delta)\,, \tag{1.6}$$

where $T_e(\tau_L) >> T_o$, $F_a = I_a \tau_L$ is the absorbed laser fluence, and $\delta = 2/\alpha$ is the skin depth.

After the laser pulse the electrons are rapidly cooled due to energy transfer to the lattice and heat conduction into the

bulk. Since the electron cooling time is very short, eq. (1.2) can be written as $T_i \sim T_e(\tau_L)t/\tau_i$ (neglecting the initial lattice temperature). The maximum lattice temperature can be estimated from the average cooling time of the electrons, $\tau_e^a \sim \tau_e / 2 = C_e^{'} T_e(\tau_L) / 2\gamma$ and is given by

$$T_i \sim T_e^2(\tau_L)\frac{C_e^{'}}{2C_i} \approx \frac{F_a\alpha}{C_i}\exp(-\alpha z). \quad (1.7)$$

Significant evaporation occurs when $C_iT_i > \rho L_v$, where ρ is the density and L_v is the specific heat of evaporation. Using (1.7), we can express the condition of strong evaporation as $F_a \geq F_{th}\exp(\alpha z)$, where $F_{th} \sim \rho L_v/\alpha$ is the threshold laser fluence with *fs* pulses. Then the ablation depth per pulse L is

$$L \approx \alpha^{-1}\ln(F_a / F_{th}). \quad (1.8)$$

Such a logarithmic dependence of the ablation depth per pulse has been confirmed by the ablation of copper in vacuum using 150 fs laser pulses (780 nm, ref. [15]) and in the ablation of highly oriented pyrolytic graphite (HOPG) with 120 fs pulses [16]. Our results show that for a 120 fs pulse the thermal penetration depth is about 139 nm [8].

2.2.2. Ultrafast Pulses in a Picosecond Scale

For a ps pulse, $\tau_e \sim 1ps < \tau_L \sim \tau_i \sim 10\text{-}100\ ps$ the energy transfer is similar to that in a *fs* scale. At times $t >> \tau_e$, $C_eT_e / t << \gamma T_e$, eq. (1.1) becomes quasi-stationary, eqs. (1.1-3) reduce to

$$\partial / \partial z(k_e\partial T_e / \partial z) - \gamma(T_e - T_i) + I_a\alpha\exp(-\alpha z) = 0 \quad (1.9)$$

$$T_i = \frac{1}{\tau_i}\int_0^t \exp(-\frac{t-\theta}{\tau_i})T_e(\theta)d\theta + T_o \quad (1.10)$$

The integral corresponds to the temperature increase of the lattice. At $t << \tau_i$, (1.10) can be simplified due to the quasi-stationary character of the electron temperature. Neglecting T_o, we get

$$T_i \approx T_e(1-\exp(-t/\tau_i)) \approx (t/\tau_i)T_e \quad (1.11)$$

It is obvious that in the *ps* regime the lattice temperature remains much less than the electron temperature. Thus the lattice temperature can be omitted in (1.9). When the condition $k_eT_e\alpha^2 << \gamma T_e$ is fulfilled (1.9) and (1.11) are very simple. The electron and lattice temperatures at the end of a ps pulse are given by

$$T_e \approx \frac{I_a\alpha}{\gamma}\exp(-\alpha z), \text{ and } T_i \approx \frac{F_a\alpha}{C_i}\exp(-\alpha z). \quad (1.12)$$

Note that the obtained lattice temperature is governed by the electron cooling time. Thus, both *fs* and *ps* regimes (1.7) and (1.12) give the same expression for the lattice temperature. This indicates that a logarithmic dependence of the ablation depth on laser fluence is also found in the *ps* regime. However, this conclusion is based on an assumption that the electron heat conduction is negligible. This is a very crude approximation since the electron heat conduction and the formation of melted zone must be related in *ps* ablation.

2.2.3. Pulses in Nanosecond and Even Longer Scales

Ablation with a longer pulse (*ns* or even longer) can be modeled with the condition $\tau_i \sim 10\text{-}100\ ps << \tau_L$. In this case, the electron and lattice temperatures have enough time to reach an equilibrium state, i.e. $T_e = T_i = T$ and (1.1- 1.3) reduce to

$$C_i\partial T / \partial t = \partial / \partial z(k_o\partial T / \partial z) + I_a\alpha\exp(-\alpha z). \quad (1.13)$$

There are many experimental and theoretical studies on the processes involved in laser heating and irradiation with long pulses [17]. In this regime the target surface is first heated to the melting point and then to the vaporization temperature. During the interaction the dominant energy loss is heat conduction into the solid target. The heat penetration depth is given by $l \sim (Dt)^{1/2}$, where $D = k_o/C_i$ is the thermal diffusivity. Note that for a long pulse, $D\tau_L >> 1/\alpha^2$. The energy deposited inside the target per unit mass is given by $E_m \sim It / \rho l$. Evaporation occurs when $E_m \sim L_v$ at t_{th}, where L_v is the specific heat of evaporation. So, the condition for strong evaporation becomes, $E_m > L_v$ (or $\tau_L > t_{th}$) and

$$I \geq I_{th} \sim \frac{\rho L_v D^{1/2}}{\tau_L^{1/2}}, F > F_{th} \sim \rho L_v D^{1/2}\tau_L^{1/2} \quad (1.14)$$

for the laser intensity and the fluence, respectively. A striking characteristic is that the threshold laser fluence depends on the square root of the laser pulse width. A deviation of the damage threshold from the $\tau^{1/2}$ scaling with short pulses is clearly evident by ablation of fused silica by infrared (1053 nm) and visible (526 nm) laser radiation [18].

In summary, *fs* pulses trigger a nonthermal ablation mechanism since both the electron-lattice thermal coupling and thermal diffusion to the lattice take longer time than the pulse width. ns pulses allow thermal equilibrium to occur between the electrons and the lattice.

2.3. Plasma Annealing Theory

Interaction between intense laser and materials leads to the formation of high density electron-hole plasmas. The plasmas characterization has been initiated by the investigation of laser annealing and nanosecond/picosecond laser-induced phase transitions in solid materials [19]. The so-called plasma model describes processes occurring in laser excited *e-h* plasmas and plasma-induced softening of the crystal lattice [18-22].

We suppose that the target fills half-space at $x > 0$, overlapped by the skin depth (optical penetration depth) $l_s = \frac{c}{\varpi k}$, where k is the imaginary part of the refractive index and ω the laser frequency. The dielectric function in the Drude approximation describes the initial solid state just before ablation:

$$\varepsilon = 1 - n_e\frac{\langle\sigma\rangle}{\omega}(i+\omega\tau_m) = 1 - \frac{\omega_{pe}^2}{\omega(\omega+i\nu_m)}, \ \varepsilon^{1/2} = n + ik \quad (1.15)$$

Here n_e is the electron density, $\omega_{pe} = (4\pi e^2 n_e / m)^{1/2}$ is the electron plasma frequency, ν_{eff} is an effective collision frequency of electrons with the lattice (ions). For normal

incidence, the absorption, reflection and transmission coefficients, *A, R*, and *T*, are given as

$$R = \left|\frac{1-\sqrt{\varepsilon}}{1+\sqrt{\varepsilon}}\right| = \frac{4\,\mathrm{Re}\sqrt{\varepsilon}}{\left|1+\sqrt{\varepsilon}\right|^2},$$

$$T = \left|\frac{2\,\mathrm{Re}\sqrt{\omega}}{1+\sqrt{\omega}}\right|,$$

$$\text{and } A = 1 - R \approx 4\,\mathrm{Re}\left(\frac{\sqrt{\varepsilon}}{|\varepsilon|}\right) \approx 2\frac{\nu}{\omega}\left(\frac{n_c}{n_e}\right)^{1/2}. \quad (1.16)$$

Here $n_c = (\pi mc^2 / e^2\lambda^2)$ is the critical density.

Laser-matter interaction can be separated into excitation and transition stages. In the former, the photoionization process is sensitive to the Keldysh parameter,

$$\gamma = \frac{\omega_e (2mU_I)^{1/2}}{eE} \quad (1.17)$$

where U_I is the zero field ionization potential, ω_e is the electron quiver frequency in the light field, E is the peak electrical field, e and m are the charge and mass of the electron, respectively. At $\gamma << 1$, the ionization process is characterized as a tunneling procedure. At $\gamma >> 1$, ionization is better modeled as a multiphoton process. Recently, the appropriate boundary of multiphoton regime is found closely to $\gamma > 0.5$ [23]. The non-resonant n^{th} order multiphoton ionization rate [24] is

$$P_i = \sigma_n \left(\frac{I}{\hbar\omega_e}\right)^n \quad (1.18)$$

where σ_N is the generalized n^{th} order cross section and I is the peak laser intensity. With increasing electron density, the second ionization mechanism, impact ionization can not be avoided. Thus, the time dependence of free electron density is defined by the rate equation [18, 25]

$$\frac{dn_e}{dt} = n_e P_{imp} + n_a P_i \quad (1.19)$$

Here n_a is the density of neutral atoms, P_{imp} is the probability for ionization by electron impact. For single ionization [25] these two probabilities can be expressed as

$$P_{imp} \approx \frac{\hbar\omega_e}{U_I}\left(\frac{2\omega^2 \nu_{eff}}{\omega^2 + \nu_{eff}^2}\right),$$

$$P_i \approx \omega n^{3/2}\left(\frac{\hbar\omega_e}{2U_I}\right)^n. \quad (1.20)$$

It is evident that the relative role of the impact and multiphoton ionization depends on the relation between the electron quiver energy and the ionization potential. For a 100 fs pulse, multiphoton ionization creates a substantial amount of free electrons. When the electron density approaches 10^{17} cm^{-3}, the collisional ionization rate begins to exceed the multiphoton ionization rate [26]. When this density approaches 10^{22} cm^{-3}, the reflectivity dramatically increases [27]. The maximum density was found to be in excess of 10^{22} cm^{-3}, which corresponded to approximately 10% of the total valence-band population [27].

A lattice softening is theoretically expected when 10% of the valence electrons are excited into the conduction band [18]. Lattice softening leads to melting, as predicted by *ab initio* molecular-dynamic calculation [28] and observed experimentally by time-resolved reflectivity [29]. Such melting is an ultrafast phenomenon and is not a consequence of conventional thermal heat transfer.

2.4. Interaction Between Ultrafast Laser Pulses and Nanoparticles

According to Two-temperature model, at the interaction period shorter than the laser pulse width, the electrons will be heated to a very high temperature while the lattice is still kept cool. Immediately after a pulse excitation, two-temperature model can be simplified as

$$C_e \frac{\partial T_e}{\partial t} = -\frac{\partial Q(z)}{\partial z} - \gamma(T_e - T_i), \quad (1.21)$$

The electron specific heat $C_e = gT_e$, where $g = \frac{\pi^2 k_B^2 f(\varepsilon_F)}{э}$.

$$C_i \frac{\partial T_i}{\partial t} = \gamma(T_e - T_i), \quad (1.22)$$

If the heat dissipation into the surrounding can be omitted, by equating the heat lost by the electrons to the heat gained by the lattice, it is straightforward to obtain the final system temperature ($T_e = T_i = T_f$)

$$T_f \approx \left(\frac{\gamma}{2C_i}\right)(T_e^i)^2 + 298 \quad (1.23)$$

where T^i_e is the initial electron temperature. Appropriate value for γ is $\gamma = 66\ Jm^{-3}K^{-2}$ for Au or 65 for Ag. $C_i = 25.42\ JK^{-1}mol^{-1} = 2.4 \times 10^6\ JK^{-1}m^{-3}$ [30]. Thus, for an initial electron temperature of 2300 K, the final tmeprature (lattice temperature) is only 370 K, lower than the melting temperature of nanoparticles at a size not smaller than 5 nm [31]. This indicates that the nanoparticles can keep the solid state after femtosecond irradiation if the laser fluence is not too high. However, it has been proven that nanoparticles display a surface melting at certain low temperature range if they are not too small [32]. It is important to mention that if nanoparticles are tiny clusters with limited atoms they may display suddenly global melting without surface melting. If we consider the heat dissipation into the surrounding, the recent simulation displays that the maximum penetration depth of heat is about 40 nm after the femtosecond laser irradiation [33]. This supports that the femtosecond laser irradiation can induce the surface melting of large nanoparticles.

3. EXPERIMENTS OF FEMTOSECOND LASER-SOLID INTERACTION

Based on the theoretical consideration described above, the interaction between femtosecond laser pulses and solid can result in versatile effects on solid state materials, such as, electron excitation, plasma generation, thermal diffusion, material ablation and shock-wave loading. The following

experiment displays that these effects mainly take place in a nanoscale depth so that femtosecond laser irradiation can be used for surface precise processing and nanowelding.

3.1. Surface Nanoengineering by Femtosecond Laser Irradiation

Fig. (**2**) shows an ablation crater created by focused laser beams on the surface of graphite. The morphology is a result of 25 overlapping pulses at energy of 700μJ/pulse. The central crater of 50 μm in diameter is surrounded by an outer region with less ablation. The surface rippling structure is obvious in this gentle ablation area. The details will be discussed later. The detailed features of the crater wall are shown in the inset of Fig. (**2**). The micro-stripes with a rough space equal to the laser wavelength are evident. More importantly, the liquid droplets can be found with a centrifugal ejection direction, indicating the melting of carbon and the effect of shock wave.

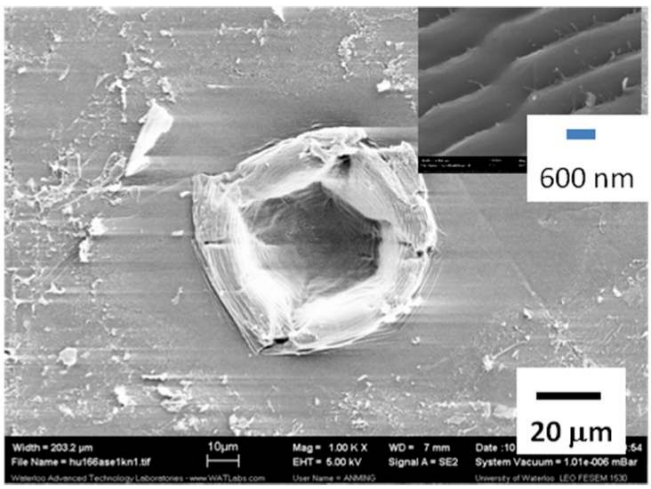

Fig. (2). Typical SEM image of highly oriented pyrolytic graphite after irradiation with 25 continuing laser pulses chain with a width of 120 fs, 700 μJ/pulse and at a wavelength of 800 nm. Inset: Local morphology of the wall of the central crater.

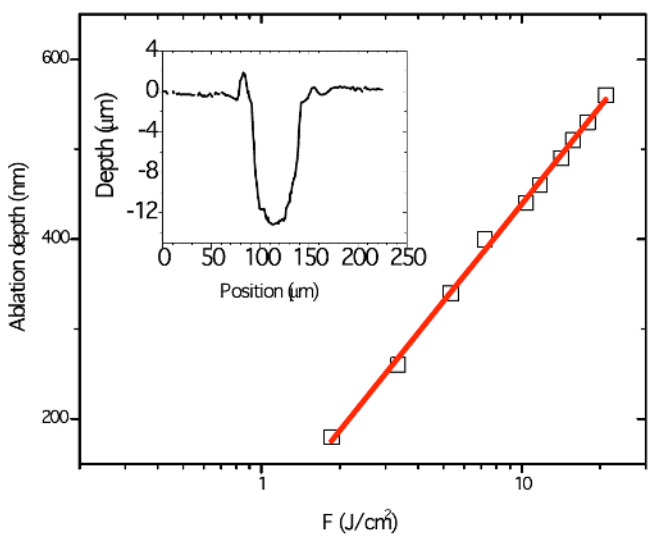

Fig. (3). Ablation depth per pulse plotted against incident fluence. The solid line corresponds to a two-temperature model. Inset: the profile of central crater generated by fs laser irradiation.

The profile of the central crater is shown in the inset of Fig. (**3**). Fig. (**3**) presents the ablation depth per pulses versus incident fluence. It is straightforward that L can be described using a two-temperature model, $L = \alpha^{-1} ln\ (F/F_{th})$, where α^{-1} is the electronic thermal penetration depth and F_{th} the damage threshold. The best fit yields α^{-1} =139 nm and F_{th} =0.41 J/cm^2 [8]. It is important to point out that the current laser intensity leads to a strong ablation, which is much larger than the intensity that generated a gentle ablation located in the vicinity of central crater.

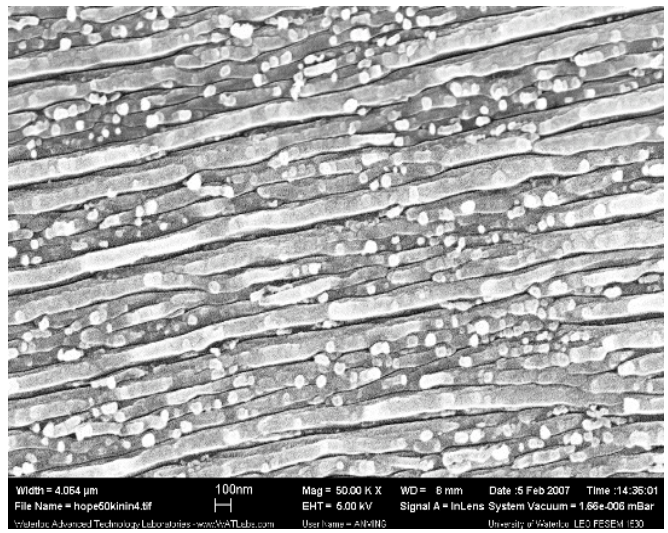

Fig. (4). Nanorippling stripes on the surface of HOPG induced by femtosecond laser irradiation.

Fig. (**2**) shows that surface defects and impurities are totally removed from these gentle ablation regions. These areas rough in a double size of central crater (strong ablation area) are smooth in a microsize roughness. Meanwhile, they display well organized structures in a nanoscale. The detailed morphology is shown in Fig. (**4**). These stripes may have formed by a self-organization processing since they have a wavelength period of about 100 nm, which is much smaller than the incident wavelength. Our further study show their orientation is coherent to the laser polarization. Thus a magnetic formation mechanism is proposed for such nanostripes.

In summary, the experiment shows that the interaction between femtosecond laser pulses and solid state materials is a nonthermal mechanism, which can be well explained by the two-temperature model. As the laser intensity is high enough it ablates the materials, leads the melting of material, and loads a shockwave impact onto the material. However, these effects are limited within a nanoscale surface penetration depth. With a lower laser intensity the irradiation results in nanoscopic fluctuation of roughness. These results show the possibility of surface nanoengineering with simple controlling of laser intensity and pulse numbers.

3.2. Femtosecond Laser-Induced Nanowelding

Fig. (**5a**, **b**) shows the 1 mM Au nanoparticle solution before and after irradiated at a laser intensity of 4x 10^{14} W/cm^2 for 10 min. As-grown Au nanoparticles (before irradiation) have an average size of 15 nm. Two effects have been observed by femtosecond laser irradiation: the

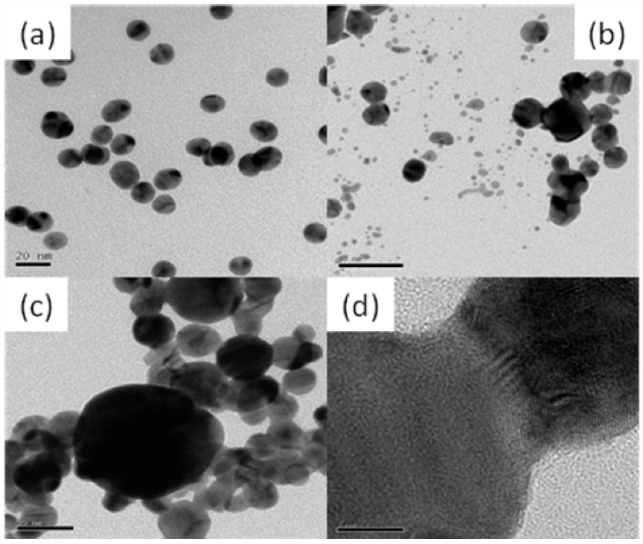

Fig. (5). shows the nanowelding of Au nanoparticles by femtosecond laser irradiation. (**a**) pristine liquid, (**b**) irradiation at an intensity of 4 x 10^{14} W/cm^2, (**c**) irradiation at 3x10^{10} W/cm^2, (**d**) local structures of typical welded necks between two particles shown in (**c**). Note that the scales are 20 nm in (**a**, **c**) and 50 nm in (**b**) and 5 nm in (**d**).

generation of large number of tiny nanoparticles with a size of 1-3 nm and welding of 2-3 Au nanoparticles with a size around 15 nm. It is reasonable to deduce that these tiny nanoparticles are created by the fragmentation of Au nanoparticles through laser irradiation. A previous study has identified the electron ejection as the first step of photofragmentation by nanosecond laser pulses [34]. This electron emission causes nanoparticles to become positively charged and the repulsion among the charges leads to the fragmentation. Compared to nanosecond laser, the interaction between femtosecond laser pulses and matter is dominant by electron ejections and there is little energy transferring between excited Au electrons and Au lattice [9]. It is thus expected that the effective photofragmentation will occur in femtosecond laser irradiation. The laser –induced breakdown of water occurs at an intensity of around 10^{12} W/cm^2 in case of the pulse width of 100 fs [35]. At present experiments, about 5 mm long filamentary area is found in Au nanoparticle solution in the vicinity of the focal point. This indicates water breakout by the focused laser in the regime. It is possible rich ions from water breakout and vibrated filaments of extremely intensive laser enhance the fragment of Au nanoparticles. This is evident in Fig. (**5c**) where only welded Au nanoparticles are observed. Besides, it is worth noting that heating-melting-evaporation processes are also observed in nanosecond laser irradiation [36]. It is difficult to attribute such a thermal mechanism for the welding of Au nanoparticles since the thermal coupling time between electrons and lattice is about 1 picosecond, remarkably longer than the laser pulses. Besides, the nanoparticles in Fig. (**5c**) keep polycrystalline indicating a non-thermal welding mechanism by femtosecond laser irradiation. Fig (**5d**) displays a high resolution TEM image of the neck region between two welded particles. The clear lattice matching evidences the fusion of two particles through rebuilding metallic bonding.

Fig. (**6**) shows SEM micrographs of the irradiation effect on Ag nanoparticle films. The film is deposited on Si wafer by dripping polymer coated Ag nanoparticles. The polymer is polyethylenimine. The average size of Ag nanoparticles is about 20 nm. The effect of polymer coating is evident: the thermal sintering is totally suppressed and Ag nanoparticles keep well separated in the film. The laser irradiation is by scanning the focused laser beam at an intensity of 3 x 10^{10} W/cm^2. After irradiation, well joined Ag nanoparticles form a 3D network. The particle size keeps roughly the same as that in the pristine sample indicating a nonthermal joining mechanism free from coarsening.

Fig. (**7**) shows the possible mechanism by laser irradiation. For a nanosecond pulse or a pulse with a longer pulse width laser thermal effect is dominant, i.e. the whole nanoparticle will be heated. Meanwhile, for a fs pulse, only the surface lattice will be heated. The surface melting will be the significant feature of fs laser irradiation. Due to this surface melting, the shape and size of nanoparticles will be kept roughly unchanged. Such phenomena is evident in Fig. (**5c**) and Fig. (**6**).

3.3. Application of Nanowelded Au for Surface Enhanced Raman Spectroscopy

Nanowelded Au/Ag nanoparticles can work as effective probe for surface enhanced Raman spectroscopy. The simulation by 3D finite element theory given in Zhang's work published in this special issue displays that welded nanoparticles possess much more hot spots in the neck area compared to individual or simply adjacent nanoparticle pairs [37]. Unlike adjacent dimmers or trimmers which are bonded by weak interaction, welded nanoparticles form strong and permanent joining, which can work as stable Raman probes for repeatable analysis.

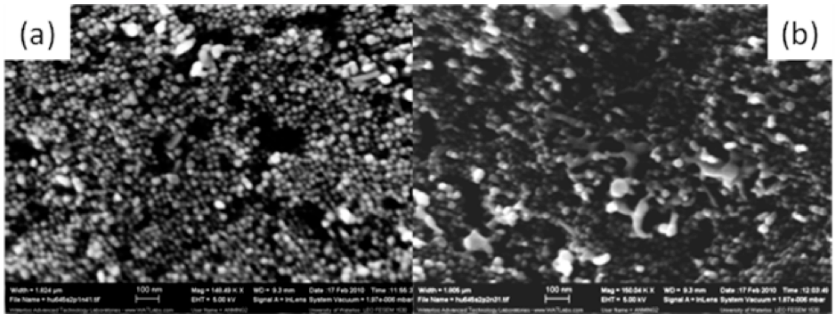

Fig. (6). Ag nanoparticle-assembled films on Si wafer (**a**) before and (**b**) after femtoseond laser irradiation.

Our previous work shows that trace polyyne molecules can be synthesized in acetone by focused femtosecond laser irradiation. These polyynes are linear carbon chains with alternative single and triple C-C bonds and different chain lengths. Their concentrations are very low so the traditional Raman spectroscopy can not detect them. Fig. (**8**) presents the surface enhanced Raman spectra of irradiated acetone with different probes. There are no features in the range of 1800 cm^{-1} to 2200 cm^{-1} while the pristine Au solution provides evidence of the weak bands, which proves the presence of polyynes. Welded Au probes display remarkably enhanced Raman activities at different frequencies in the range of 1800 cm^{-1} to 2200 cm^{-1}, which confirms the existence of polyynes with variable chain lengths.

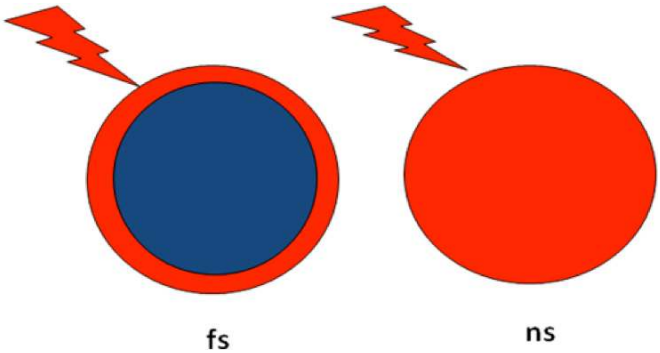

Fig. (7). Thermal effect of nanoparticles by laser irradiation with different pulse widths.

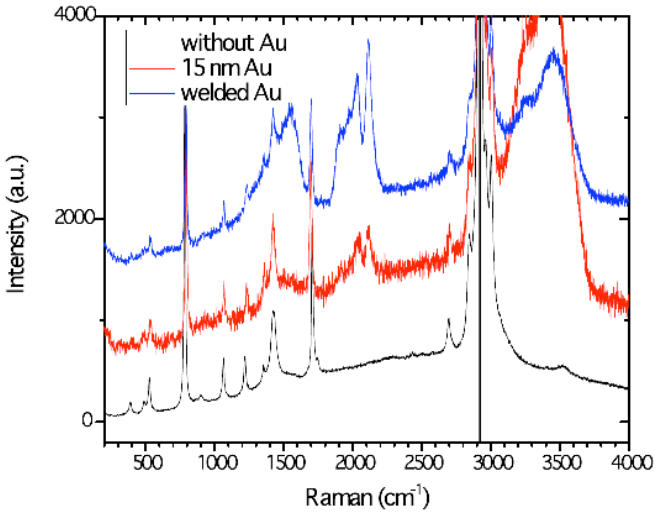

Fig. (8). Enhanced Raman spectroscopy of irradiated Acetone by femtosecond laser irradiation.

4. CONCLUSIONS AND OUTLOOK

The fundamentals of the interactions between femtosecond laser pulses and solid state materials and nanoparticles are discussed. Nonthermal surface melting is evident, which can be used for nanowelding. Welded Au nanoparticles can work as effective Raman probes for surface enhanced Raman spectroscopy. Recently, nanojoined Ag nanowires have displayed the application for a plasmon routers in integrated nanophotonics and light telecommunication [38]. Since nanowelding by femtosecond laser irradiation is an advanced manufacturing and assembling technique it is expected that further development in this field can facilitate the nanofabrication of the novel nanodevices and multifunctional molecular systems.

REFERENCES

[1] Halperin WP. Quantum size effects in metal particles. Rev Mod Phys 1986; 58: 533-603.
[2] Pelton M, Aizpurua J, Bryant G. Metal-nanoparticle plasmonics. Laser Photo Rev 2008; 2: 136-59.
[3] Khlebtsov N, Dykman LA. Optical properties and biomedical applications of plasmonic nanoparticles. J Quant Spec Rad Trans 2010; 111: 1-35.
[4] Besner S, Meunier M. Laser precision microfabrication. Springer Series in Materials Science 2010; 135: 163-87.
[5] BBC Research. Nanostructured materials for the biomedical, pharceutical, & cosmetic markets. NAN017D 2007.
[6] Lal S, Link S, Halas NJ. Nat Photonics 2007; 1: 641.
[7] Zhang ZX, Hu A, Zhang T, Xue XJ, Wen JZ, Duley WW. Subwavelength plasmonic waveguides based on ZnO nanowires and nanotubes: a theoretical study of thermo-optical properties. Appl Phys Lett 2010; 96: 0431091-3.
[8] Hu A, Rybachuk M, Lu Q –B, Duley WW. Direct synthesis of sp-bonded carbon chains on graphite surface by femtosecond laser irradiation. Appl Phys Lett 2007; 91: 1319061-3.
[9] Hu A, Panda SK, Khan MI, Zhou Y. Laser welding, microwelding, nanowelding and nanoprocessing. Chin J Lasers 2009; 36: 3149-59.
[10] Zhou Y. Microjoining and nanojoining. Cambridge, England: Woodhead publishing Ltd. CRC Press 2008.
[11] von der Linde D, Sokolowski-Tinten K, Bialkowski J. Laser-solid interaction in the femtosecond time regime. Appl Surf Sci 1997; 110: 1-10.
[12] Kaganov M I, Lifshitz I M, Tanatarov LV. Sov Phys JETP 1957; 4: 173.
[13] Anisimov SI, Kapeliovich BL, Perel'man TL. Sov Phys JETP 1974; 39: 375.
[14] Chichkov BN, Momma C, Nolte S, von Alvensleben F, Tunnermann A. Femtosecond, picoseconds and nanosecond laser ablation of solids. Appl Phys A 1996; 63: 109-15.
[15] Momma C, Nolte S, Chichkov BN, Alvensleben FV, Tunnermann A. Precise laser ablation with ultrashort pulses. Appl Surf Sci 1997; 109/110: 15-9.
[16] Shirk MD, Molian PA. Ultra-short pulsed laser ablation of highly oriented pyrolytic graphite. Carbon 2001; 39: 1183-93.
[17] Duley WW. UV lasers: Effects and applications in materials science. Cambridge: Cambridge University Press 1996.
[18] Perry M D, Stuart B C, Banks PS, Feit MD, Yanovsky V, Rubenchik AM. Ultrashort-pulse laser machining of dielectric materials. J Appl Phys 1999; 85: 6803-10.
[19] Van Vechten JA, Tsu R, Saris FW, Hoonhout D. Reasons to believe pulsed laser annealing of Si does not invole simple thermal melting. Phys Lett 1979; 74A: 417-21.
[20] Stampfli P, Bennemann KH. Phys Rev B 1990; 42: 7163-73.
[21] Silvestrelli PL, Alavi A, Parrinello M, Frenkel D. Structural, dynamical, electronic, and bonding properties of laser-heated silicon: An ab initio molecular-dynamics study. Phys Rev B 1997; 56: 3806-12.
[22] Gamaly EG, Rode AV, Luther-Davies B, Tikhonchuk VT. Ablation of solids by femtosecond lasers: ablation mechanism and ablation thresholds for metals and dielectrics. Phys Plas 2002; 9: 949-57.
[23] Ilkov FA, Decker JE, Chin SL. Ionization of atoms in the tunnelling regime with experimental evidence using Hg atoms. J Phys B Opt Phys 1992; 25: 4005-20.
[24] Gontier Y, Trahin M. Multiphoton ionization of atoms. Ed. Chin SL, Lambropoulos P, Academic New York 1984.
[25] Il'insky YA, Keldysh LV. Electromagnetic response of materials media. New York: Plenum 1994.
[26] Stuart BC, Feit MD, Herman S, Rubenchik AM, Shore BW, Perry MD. Nanosecond-to-femtosecond lasr induced breakdown in dielectrics. Phys Rev B 1996; 53: 1749-61.
[27] Sokolowski-Tinten K, Blome C, Dietrich C, Tarasevitch A, Horn von Hoegen M, von der Linde D. Femtosecond X-ray measurement of ultrafast melting and large acoustic transients. Phys Rev Lett 2001; 87: 225701-3.
[28] Silvestrelli P L, Alavi A, Parrinello M, Frenkel D. Ab initio molecular dynamics simulation of laser melting of silicon. Phys Rev Lett 1996; 77: 3149-52.

[29] Reitze DH, Ahn H, Dower MC. Optical properties of liquid carbon measured by femtosecond spectroscopy. Phys Rev B 1992; 45: 2677-93.

[30] Hodak JH, Martini I, Hartland GV. Spectroscopy and dynamics of nanometer-sized noble metal particles. J Phys Chem B 1998; 102: 6958-67.

[31] Zhao S, Wang S, Ye H. Size-dependencet melting properties of free silver nanoparticles. J Phys Soc Jpn 2001; 70: 2953-7.

[32] Hu W, Xiao S, Yang J, Zhang Z. Melting evolution and diffusion behaviour of vanadium nanoparticles. Eur Phys J B 2005; 45: 547-54.

[33] Garwe F, Bauerschafer U, Csaki A, *et al*. Optically controlled thermal management on the nanometer length scale. Nanotechnology 2008; 19: 0552071-12.

[34] Hu A, Sanderson J, Zaidi AA, *et al*. Direct synthesis of polyyne molecules in acetone by dissociation using femtosecond laser irradiation. Carbon 2008; 46: 1792-28.

[35] Kennedy PK, Hammer DX, Rockwell BA. Laser-induced breakdown in aqueous media. Prog Quant Electr 1997; 21: 155-248.

[36] Nolte S, Momma C, Jacobs H, *et al*. Ablation of metals by ultrashort laser pulses. J Opt Soc Am B 1997; 14: 2716-22.

[37] Zhang T, Zhang X Y, Hu A. Plasmonic properties of welded metal nanoparticles. Open Surf Sci J 2011; 3: 000-000.

[38] Fang Y, Li Z, Huang Y, *et al*. Branched silver nanowires as controllable Plasmon routers. Nano Lett 2010; 10: 1950-4.

Received: November 16, 2010 Revised: January 10, 2011 Accepted: January 12, 2011